Hindawi Publishing Corporation
International Journal of Antennas and Propagation
Volume 2013, Article ID 173286, 10 pages
http://dx.doi.org/10.1155/2013/173286

Research Article

Application of Asymptotic and Rigorous Techniques for the Characterization of Interferences Caused by a Wind Turbine in Its Neighborhood

Maria Jesús Algar, Lorena Lozano, Javier Moreno, Iván González, and Felipe Cátedra

Computer Sciences Department, University of Alcalá, 28871 Alcalá de Henares, Spain

Correspondence should be addressed to Maria Jesús Algar; chus.algar@uah.es

Received 11 October 2012; Revised 8 January 2013; Accepted 15 January 2013

Academic Editor: David de la Vega

This paper presents a complete assessment to the interferences caused in the nearby radio systems by wind turbines. Three different parameters have been considered: the scattered field of a wind turbine, its radar cross-section (RCS), and the Doppler shift generated by the rotating movements of the blades. These predictions are very useful for the study of the influence of wind farms in radio systems. To achieve this, both high-frequency techniques, such as Geometrical Theory of Diffraction/Uniform Theory of Diffraction (GTD/UTD) and Physical Optics (PO), and rigorous techniques, like Method of Moments (MoM), have been used. In the analysis of the scattered field, conductor and dielectric models of the wind turbine have been analyzed. In this way, realistic results can be obtained. For all cases under analysis, the wind turbine has been modeled with NURBS (Non-Uniform Rational B-Spline) surfaces since they allow the real shape of the object to be accurately replicated with very little information.

1. Introduction

In the last decade, the interest in renewable energy has increased as a consequence of the climate change and the diminishing of fossil fuel. In particular, the use of wind turbines as electric generators has grown about 20% annually [1] because wind turbines create cost-effective and nonpolluting energy. In the process of generating electric energy the kinetic power from the blades is converted into electricity within the turbine. Following this procedure, a single wind turbine usually generates a few MW of clean energy. Historically, the turbines were used to run machinery; however, nowadays these devices are used to produce electric power from wind power. In this way, the amount of generated power depends entirely on the amount of wind in the area where the wind turbine is located. Therefore, in terms of clean energy, wind turbines are very useful. Nonetheless, the presence of these devices creates problems related to electromagnetic interferences, which represent the main focus of interest in this work.

The aspect of wind turbines is quite characteristic. They are made up of a tower and three blades joined by a rotor. The size of these structures is usually very large. The height of the tower is around 80 meters and the length of the blades is around 40 meters. Hence, the total height of the wind turbine is around 120 meters. It must be considered that the shape of the tower is not a cylinder since its diameter is larger at the bottom than at the top. As a result of their large dimensions, they can interfere with many services such as TV broadcast [2–4], radar communications, VHF or UHF transmissions, aerial radio navigation systems, and meteorological radar systems. Therefore, before installing a wind farm, a study of the potential impact of wind turbines in electromagnetic applications must be carried out to avoid any possible interference.

Many of these effects have been extensively introduced in the previous literature. For instance, the EM scattering of different scaled models for wind turbines is characterized in [5]. Twenty-eight years ago, an interesting study about interferences with television was presented in [3]. More recently,

for the evaluation of problems caused on TV broadcast, the International Telecommunication Union (ITU-R) published in 1992 the recommendation ITU-R BT.805 [6], about the interferences in analog television, and in 2011 the ITU-R BT.1893 [7], about the impairment caused to digital television.

The large size and rotational movement of the turbine blades produces a shift on the frequency of electromagnetic signals. This causes serious distortion on telecommunication systems. For this reason, it is quite interesting to study the Doppler features of wind turbines [8–10]. In this way, the US. Department of Defense undertook a rigorous measurement campaign to provide information about the interference issues caused by these devices in civilian and military radar systems [10]. The main purpose was to predict and measure the RCS and Doppler signature of a typical wind turbine.

In this paper, three different analyses have been conducted to study the effects caused by a wind turbine in telecommunication systems located in its neighborhood.

(i) Scattered field: to implement this kind of analysis, both high-and-low frequency techniques, such as GTD/UTD and MoM, respectively, have been used. Nevertheless, due to the tremendous size of this kind of structure [11–14], the application of MoM is limited only to low frequencies. Thus, PO and an hybridized MoM-PO approximation have been used to perform simulations of huge structures at high frequencies.

(ii) Radar cross-section: for the purpose of analyzing the RCS of a wind turbine, MoM is applied too. In the group of asymptotic techniques, several studies such as [15, 16] the use of Physical Optics (PO) solutions for the computation of RCS. Nonetheless, this previous research does not take into account multiple reflections and surface wave propagation. Consequently, a method based on the combination of Geometrical Optics (GO) and PO has been applied to consider multiple interactions between the facets of the wind turbine [17].

(iii) Doppler spectra: as in the analysis of the scattered field, UTD, MoM, and MoM-PO have been used to compute the Doppler shift caused by a wind turbine.

For all these cases, the geometrical model plays an important role. The structure under study is modeled using parametric surfaces, Non-Uniform Rational B-Spline (NURBS) [18, 19]. This lets us build an accurate representation of the real object.

All the analyses here presented have been performed with NewFasant [20], a computer tool for electromagnetic analysis and design. Before starting any analysis, the geometrical model must be meshed. The mesher included on NewFasant has been used, considering different mesh sizes depending on the simulation frequency.

This paper is organized as follows: Section 2 provides an overall description of different techniques applied to analyze the scattered field, along with some test cases. The techniques applied to analyze the RCS of a wind turbine are the focus of Section 3. Section 4 presents methods to compute the Doppler spectrum of a wind turbine and some results. Finally, Section 5 summarizes the conclusions of this study about wind turbines.

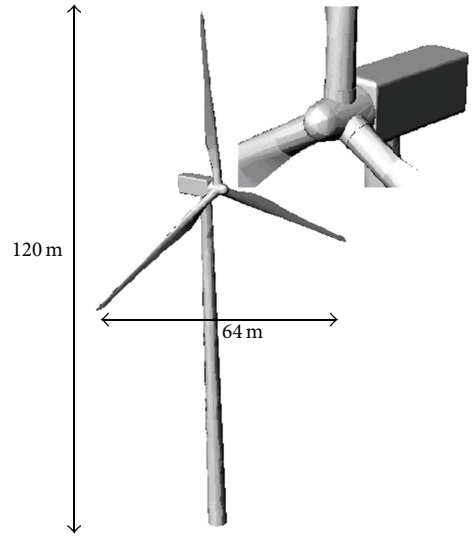

Figure 1: Geometrical model of a wind turbine.

2. Scattered Field of a Wind Turbine

As mentioned above, this paper presents several analyses to characterize the interferences caused by a wind turbine on radio systems located in its vicinity. This section shows the study of the scattered field of a wind turbine, in which the ground reflection has not been taken into account, considering the object as a static one.

Before starting the computation of the scattered field of a wind turbine or any other analysis, it is necessary to follow some initial steps. First, the geometrical model of the object must be obtained. As it has been mentioned in Section 1, to perform this step, NURBS surfaces have been used. In Figure 1, the geometrical model used in these studies is shown, a wind turbine of 120 m height and 64 m between the extremities of its blades. This model is composed of 1009 parametric surfaces.

Frequently, a simplified model of a wind turbine is created considering that it is only composed of perfect conductors. This model is itself very interesting because it is considered a worst case for system analyses. However, a real model of a wind turbine must be generated considering that the blades are composed of different dielectric materials with two plates inside them to provide rigidity to the structure, as shown in Figure 2.

Hence, to perform the analysis of the test case of these two models, Figure 3 shows the scenario considered. The main goal of this scenario is to model the real situation between a transmitter, which is far from the wind turbine and a receiver, which can be near from the wind turbine. Therefore, 360 observation points have been distributed over a circle of radius of 5 km, centred in the wind turbine, and elevated 60 m of above the reference plane ($z = 0$). The feeding antenna is a vertical dipole oriented along the z-axis, which radiates

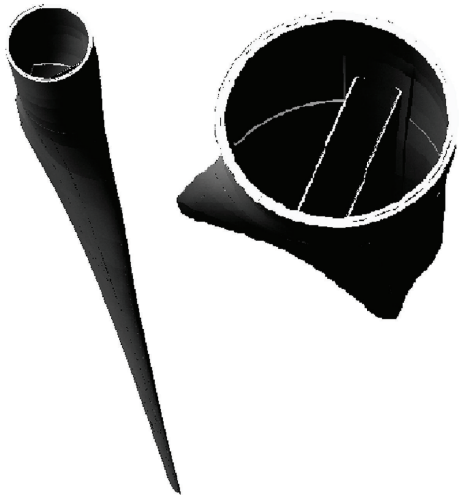

Figure 2: Dielectric model of a blade.

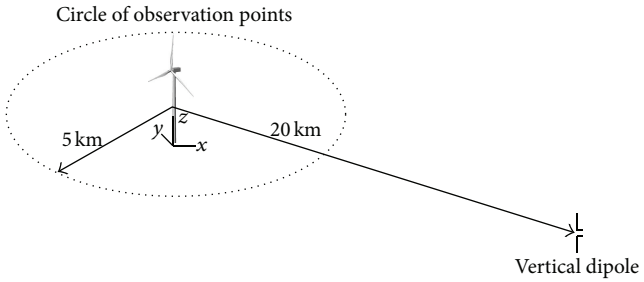

Figure 3: Description of the scene for the analysis of the scattered field.

2.15 Kw. It has been located 20 km far away from the wind turbine and with the same elevation than the observation points.

Two different geometrical models of the wind turbine have been compared.

(i) The first model is a turbine made of conductor, exclusively. We call it conductor model.

(ii) The second one is a turbine with a metallic tower and with its blades made of a dielectric material, to consider the case of a real turbine which is not only composed of conductor. We call it dielectric model.

For both models, three different techniques have been applied.

(i) MoM, a rigorous technique that tries to solve directly the Maxwell equations by dividing the geometry in small parts [21]. The efficiency of this technique has been improved thanks to the inclusion of an advanced version of the Multilevel Fast Multipole Method, Characteristic Basis Function Method, and a Domain Decomposition procedure [22, 23]. This approach can be applied to all frequencies.

(ii) PO and MoM-PO solutions have been included to speed up the computation of the electrical field when the simulation is performed at high frequency. In the MoM-PO solution, the current on the metallic parts of the wind turbine is obtained using MoM and ignoring the dielectric parts of the turbine. The equivalent-induced current in the dielectric parts is computed using PO considering the incident field and the field due to the currents on the metallic parts.

(iii) Uniform Theory of Diffraction (UTD), an asymptotic technique introduced by Pathak and Kouyoumjian in [24, 25]. It is an extension of the Geometrical Theory of Diffraction (GTD) [26, 27] in order to predict diffraction in transition regions, where the value provided by GTD for the electrical field is infinite [28]. As the requirements in terms of CPU time and memory resources of the ray-tracing techniques are too high, the combination of the Angular Z-buffer (AZB), the Space Volumetric Partitioning (SVP), and A* heuristic search method has been applied [29]. Likewise, this combination allows multiple interactions between different parts of the object to be treated in order to attain more accurate results.

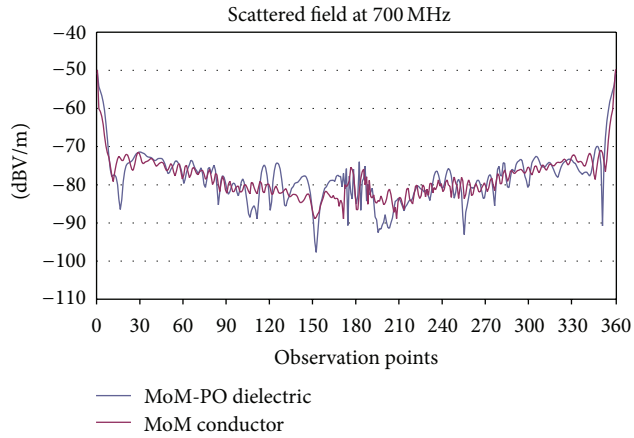

Figure 4: Comparison of the scattered field at 700 MHz between the conductor and dielectric models.

For the computation of the scattered field at the observation points shown in Figure 3, MoM has been applied for the conductor model and the MoM-PO approximation for the dielectric model. Figures 4 and 5 show the comparison of results obtained at 700 MHz and 1300 MHz, respectively.

As shown in Figures 1, 2, 3, 4, and 5, the scattered field obtained in the analysis of the dielectric model is higher than that obtained using the conductor model. These results are due to a shift close to 180° between the electrical field due to the tower and the electrical field due to the blades in the case of the conductor model.

To obtain the electrical field scattered by the wind turbine applying rigorous techniques, we shall obtain first the induced currents on the geometry. Figure 6 shows the current density on the wind turbine for the simulation at 1300 MHz for the conductor case.

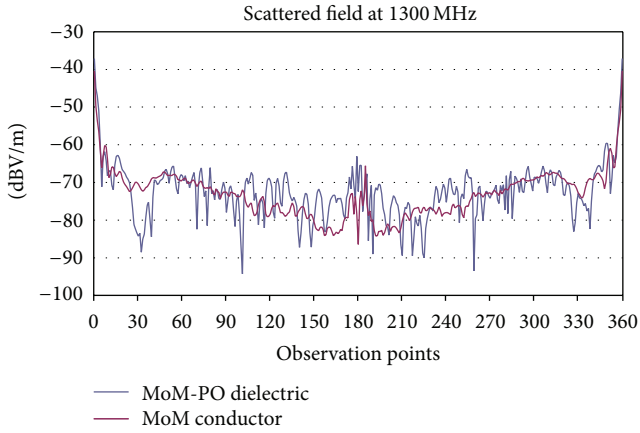

Figure 5: Comparison of the scattered field at 1300 MHz between the conductor and dielectric models.

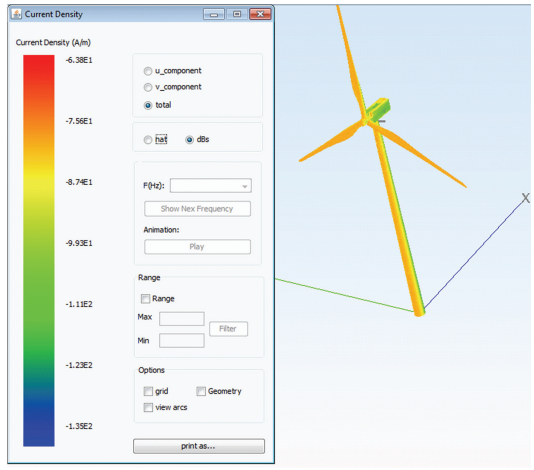

Figure 6: Current density on the wind turbine at 1300 MHz.

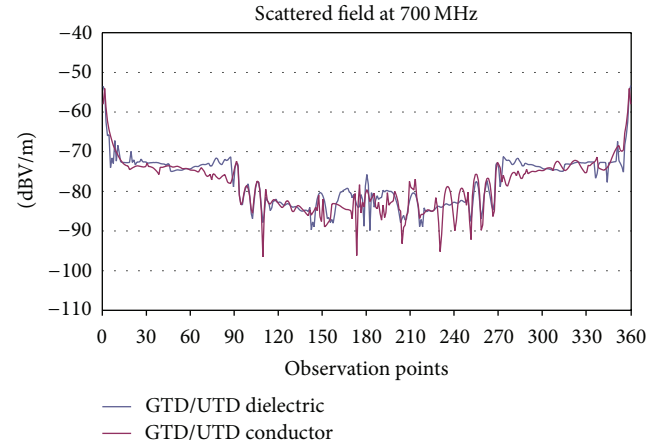

Figure 7: Comparison of the scattered field at 700 MHz between the conductor and dielectric models.

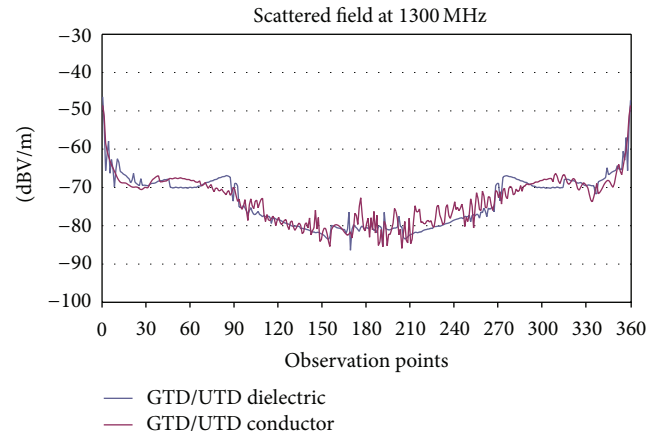

Figure 8: Comparison of the scattered field at 1300 MHz between the conductor and dielectric models.

Additionally, both models have been analysed applying the GTD/UTD technique at 700 MHz and 1300 MHz obtaining the results presented in Figures 7 and 8, respectively.

From Figures 4, 5, 7 and 8, it can be concluded that the results are very similar for both models. However, the results predicted for the dielectric model are more realistic than the results provided by the conductor model because in the first case the tower and blades have been built taking into account the actual combination of conductor and dielectric materials. In the same way, it is inferred that the tower constitutes the largest source of scattering, followed by the blades of the wind turbine. This aspect can be appreciated in the ray-tracing representation of Figure 9. The ray-tracing for two observation points has been plotted. Note that the position of the source and the observation points have been chosen close to the geometry, only to make the visualization of the ray-tracing easier.

To compare the analysis performed by MoM and GTD/UTD, Figures 10 and 11 present the differences between the scattered field obtained with both techniques at 700 MHz and 1300 MHz, respectively, considering the conductor model of the wind turbine.

As it can be observed from Figures 10 and 11, the graphics obtained at 1300 MHz are more similar than the graphics obtained at 700 MHz. Hence, at low frequencies, the results of GTD/UTD and MoM present some differences because there are some parts of the wind turbine which are electrically too small for the asymptotic technique to provide accurate values for the electrical field.

Considering the dielectric model of the wind turbine, the scatter field obtained with MoM-PO and GTD has been compared in Figures 12 and 13 at 700 MHz and 1300 MHz, respectively.

As it can be observed from Figures 12 and 13, the results provided by MoM-PO present more variations than the results provided by GTD. The MoM-PO approximation, after computing the induced currents on the blades, applies the PO radiation integral to reflection coefficient to these currents and obtain the fields in all directions. However, GTD only considers reflection ray for each observation direction without taking into account transmission rays. Therefore,

Table 1: CPU time and memory requirements for the scatter field of the conductor model.

	GTD/UTD (8 processors)		MoM (8 processors)	
	700 MHz	1300 MHz	700 MHz	1300 MHz
CPU time	8 min. 18 s.	8 min. 18 s.	1 h. 3 min. 45 s.	1 h. 8 min. 5 s
Memory resources	538 KB	538 KB	723 MB	2.5 GB

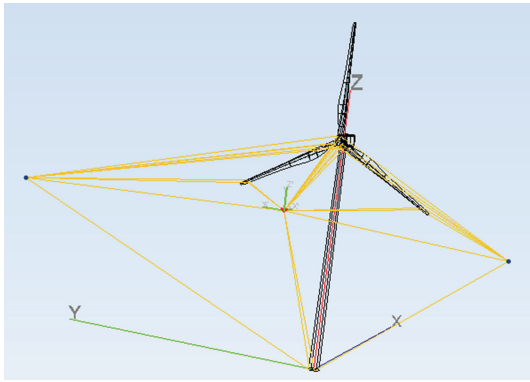

Figure 9: Ray-tracing representation for two observation points.

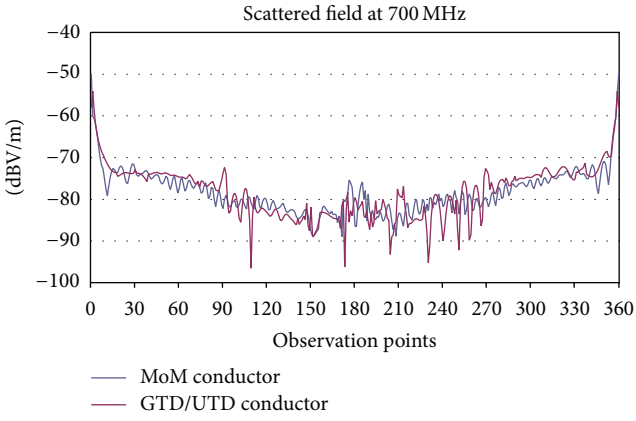

Figure 10: Comparison of the scattered field at 700 MHz between MoM and GTD/UTD.

in this case, the GTD prediction is less accurate than the MoM-PO prediction.

Nonetheless, the CPU time and memory resources required by GTD/UTD are less than in the case of MoM. Table 1 shows the comparison of these two parameters for both techniques when the scattered field of the conductor model is analyzed. The simulations of this model have been performed in a 2.0 GHz Quad Intel Xeon with 24 GB of RAM.

Table 2 presents the parameters corresponding to the analysis performed considering the dielectric model. In this case, these simulations have been performed in a 2.69 GHz QuadCore AMD Opteron with 256 GB of RAM.

Table 2: CPU time and memory requirements for the scattered field of the dielectric model.

	GTD/UTD (16 processors)		MoM (16 processors)	
	700 MHz	1300 MHz	700 MHz	1300 MHz
CPU time	14 min. 35 s.	14 min. 35 s.	2 h. 18 min. 4 s.	7 h. 13 min. 7 s.
Memory resources	382 KB	382 KB	520 MB	1.9 GB

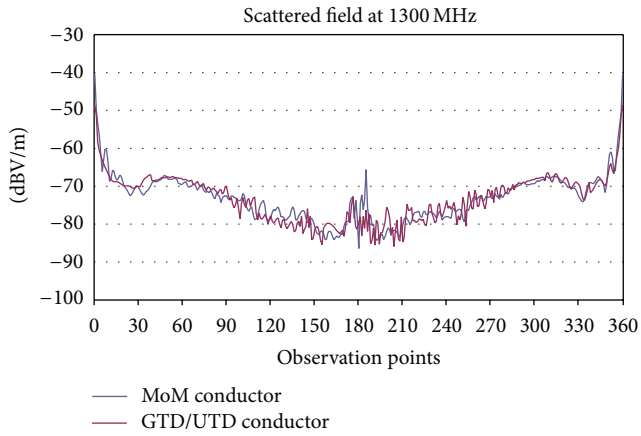

Figure 11: Comparison of the scattered field at 1300 MHz between MoM and GTD/UTD.

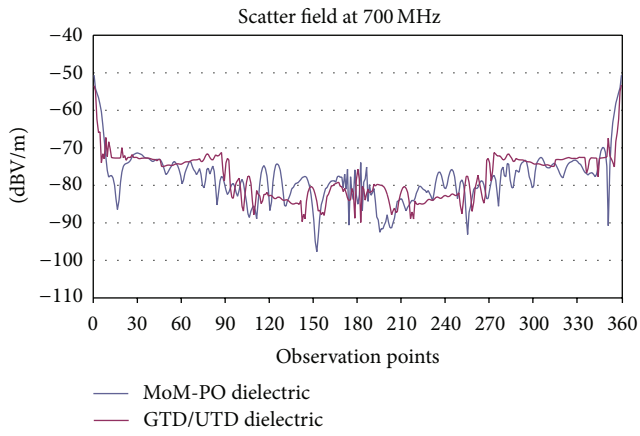

Figure 12: Comparison of the scattered field at 700 MHz between MoM-PO and GTD/UTD.

3. RCS of a Wind Turbine

The second analysis presented in this paper is the study of the RCS of a wind turbine to characterize the impairment caused to services like meteorological radar or aerial radio navigation systems. As in the scattered field case, there are numerous techniques to perform this kind of analysis. These can be classified in two different groups.

(i) High-frequency techniques these techniques are applied to analyze electrically large bodies. Techniques such as Geometrical Optics (GO) [30] and

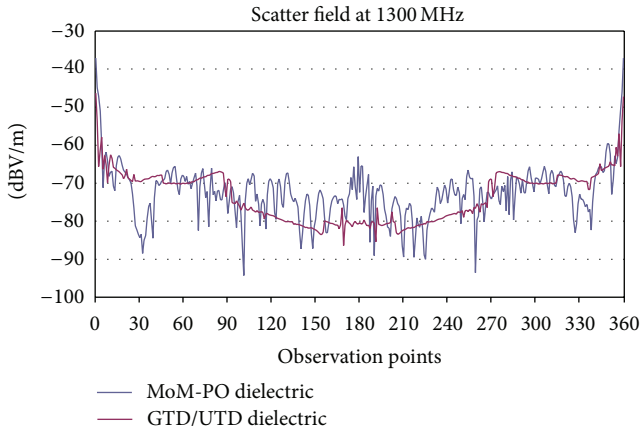

Figure 13: Comparison of the scattered field at 1300 MHz between MoM-PO and GTD/UTD.

Physical Optics (PO) [31] can be featured within this group. PO is the most common method used to compute RCS. Nevertheless, if the diffraction effect is considered, it is necessary to apply other techniques such as Equivalent Currents Method (ECM) [32]. This method lets the diffraction to be obtained at all observation directions and improves the accuracy of results for the computation of the RCS in real scenarios.

In this section, a hybrid method combining GO and PO [17] has been applied, to take into account the multiple effects among the different parts of the target. Besides, the computation time of the process to obtain the RCS has been reduced with an algorithm based on the fusion of the angular Z-buffer (AZB), the Space Volumetric Partitioning (SVP), and the depth-limited search method [33].

(ii) Rigorous techniques, such as Method of Moments (MoM) [21], which has already been introduced in Section 2.

The bistatic RCS of the metallic wind turbine has been computed applying PO and MoM at the same frequency, 1300 MHz. The results obtained by these two methods, for the cut $\theta = 90^\circ$ and a sweep from $\varphi = 0^\circ$ to $\varphi = 360^\circ$ with 361 directions, are presented in Figure 14. This simulation has been done considering reflection and diffraction effects and an incidence wave defined by $\theta = 90^\circ$, $\varphi = 180^\circ$.

From the graphic presented in Figure 14, it is inferred that the results obtained by the asymptotic and the rigorous methods are very similar. Nevertheless, a difference regarding CPU time and memory requirements exists. As shown in Table 3, the time spent by PO to perform the bistatic RCS is quite less than the time consumed by MoM. The same happens with memory requirements.

In Figure 15, a 3D representation of the RCS is displayed, using a color scale, together with the wind turbine geometry for the results obtained by MoM.

As in the analysis of the scattered field applying MoM, this technique calculates the currents on the metallic wind turbine

Table 3: CPU time and memory requirements for the calculation of the bistatic RCS.

	PO (8 processors)	MoM (8 processors)
CPU time	11 min. 41 s.	1 h. 32 min. 9 s.
Memory	123 MB	3 GB

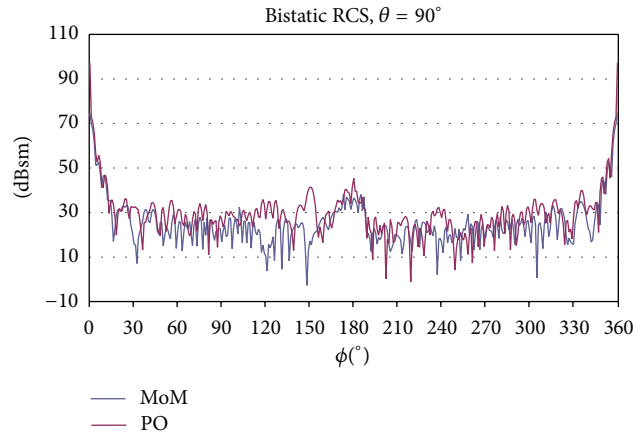

Figure 14: Comparison between the results obtained applying PO and MoM for the bistatic RCS at 1300 MHz (dBsm: decibel measure of the RCS of the target relative one square meter).

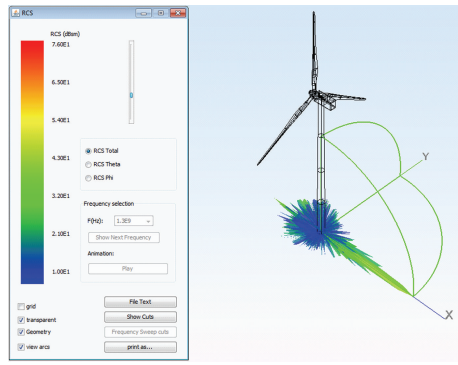

Figure 15: 3D representation of the RCS of the wind turbine at 1300 MHz applying MoM.

to compute its RCS. Figure 16 shows the current density on the wind turbine at 1300 MHz.

Finally, the scatter map of the metallic wind turbine at 3 GHz has been obtained applying PO, since this analysis lets the parts with a higher contribution to the RCS to be identified. The results for the monostatic case for the incidence angle $\varphi = 0^\circ$ and $\theta = 90^\circ$ are shown in Figure 17, where it is clear that the largest source of scatter is the tower and the blades, which are colored in red.

The computation of the bistatic RCS and the scatter map have been run in a 2.0 GHz Quad Intel Xeon with 24 GB of RAM. Only two processors have been used for the scatter map computation.

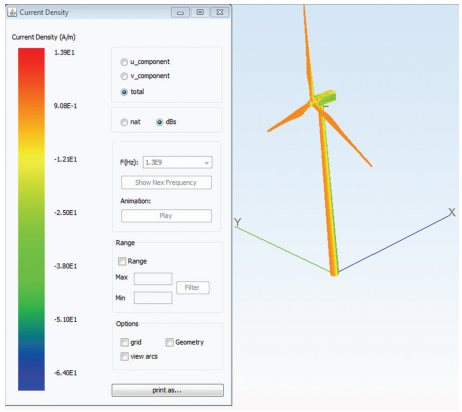

FIGURE 16: Current density on the wind turbine at 1300 MHz applying MoM.

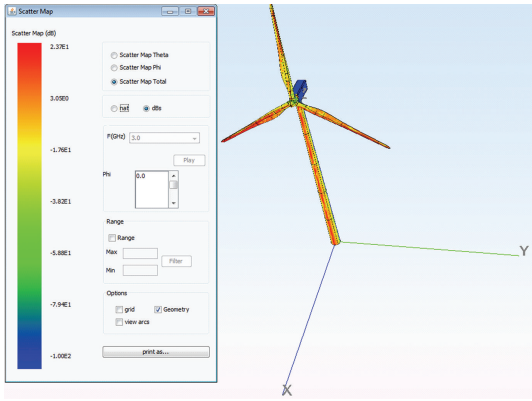

FIGURE 17: Scatter map of a wind turbine at 3 GHz.

4. Doppler Spectrum of a Wind Turbine

One of the main interference problems in the deployment of wind turbine farms in the vicinity of radio communication systems is due to Doppler frequency spectrum spreading and Doppler frequency shift generated by the rotation of the blades. In this way, the third and last analysis presented in this paper is the study of the Doppler spectra. The analysis of this effect is quite interesting since the detection of moving targets, such as planes, can be interfered by this movement. Moreover, the information provided by Doppler spectra can be used in target identification applications [10, 34, 35].

Therefore, an efficient method has been developed for both asymptotic techniques, like GTD, as rigorous techniques, like MoM, to compute the Doppler spectrum of the scattering of wind turbines. This new method has been implemented following these steps: read input data, set linear velocity, and compute the Doppler frequency. With this approach it is easier to obtain the Doppler shift generated by a moving target or by some moving parts of a target.

The first step to obtain the Doppler spectrum is to compute the linear velocity of points of the rotating parts of the wind turbines, in this case the blade. This speed in a given point is computed as follows:

$$\vec{v}_{\text{lineal}} = \vec{\omega} \times \vec{r}, \tag{1}$$

where $\vec{\omega}$ is the rotation velocity, and $\vec{r}$ is a vector normal to the rotation axis that joins the axis with the point.

Once the linear velocity has been calculated, it is very simple to obtain the Doppler frequency shift due to the linear speed of the point using the following expression:

$$f_D = f_0 \frac{v_t}{c}, \tag{2}$$

where f_0 is the simulation frequency, c is the speed of light, and v_t is the relative speed of the point that can be computed according to

$$v_t = \frac{\partial (d_1 + d_2)}{\partial t}, \tag{3}$$

where d_1 is the length of a straight path from the source to the point and d_2 is the length of the straight path from the point to the observation point. It can be noticed that these lengths are time functions that depend on the linear speed of the point.

We obtain the Doppler spectrum using MoM or PO considering a filter of 1.0 Hz of bandwidth, say we split the frequency band in windows (bins) of 1.0 Hz of width. The total field in a given frequency bin is due to all the MoM or PO subdomains that in accordance with (2) contribute in this frequency bin. The complex amplitude of the field of a MoM subdomain that contributes in this bin is computed assuming static subdomain. In this way, we obtain a complex spectral response that represents the Doppler frequency shift.

Using GTD, the complex spectral response is obtained as a discrete series of impulses, each impulse due to a ray-path. The frequency of each impulse is computed considering the reflection/diffraction point to obtain the Doppler shift in (2). The amplitude of the impulse is given by the corresponding reflection/diffraction coefficient assuming static point.

The differences between the spectral responses of MoM and GTD are due to the fact that in GTD, the spectral response is a series of impulses, each one of them associated to a reflection or diffraction point over the wind turbine, while in MoM the spectral response is computed considering the contribution of each MoM subdomain of the induced currents on the wind turbine. Each impulse of the GTD spectral response is due to the current in a surface around the reflection/diffraction point that gives the reflected/diffracted value. This surface can be large in terms of wavelengths. The GTD impulse is located in a single frequency bin. For the current in the same area, the MoM computes for each subdomain (that is electrically small) its contribution to the spectral response; therefore, the spectral response, appears "nearly" a continuous function because there will be contribution in all the bins around the bin in which the GTD impulse is located. Speaking roughly, the GTD

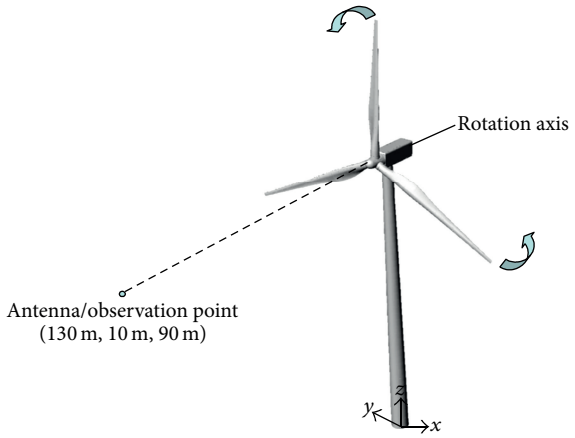

Figure 18: Description of the scene for the analysis of the Doppler spectra.

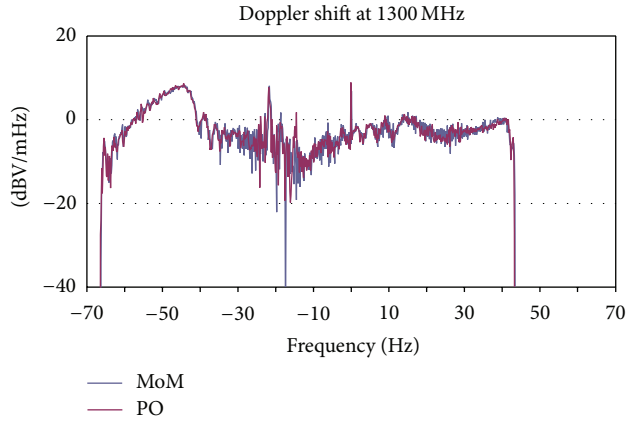

Figure 19: Comparison between the results obtained applying MoM and PO approximation for the Doppler spectra of a wind turbine.

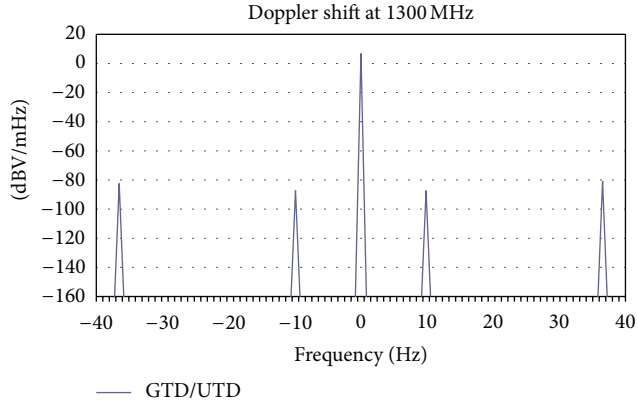

Figure 20: Doppler spectra of a wind turbine applying GTD/UTD.

approach could be equivalent to make a filtering of the MoM complex spectral response, making a filtering around the bin associated to each reflection/diffraction point. From the previous explanation it is obvious that the MoM solution is quite more accurate.

It is important to realize that with the algorithm presented above, the Doppler spectra of a wind turbine considering several rotation axes can be analysed. In this way, for each axis the surfaces rotating around it must be associated to that axis. Then, this previous formulation will be applied for each group of surfaces and rotation axis to obtain the Doppler frequency for each of them.

The scenario shown in Figure 18 presents an interesting case for the analysis of the Doppler effect of the wind turbine locating the transmitting and observation points in the same place. The geometrical model of the wind turbine is the same as in previous studies (Figure 1). However, in this case, the rotation movement of the blades with an angular speed of 2.0 rad/s around the rotor has been taken into account. The rotation axis is defined by points (7.27 m, 0.0 m, 79.38 m) and (−21.193 m, 0.0 m, 81.87 m). The transmitting and observation points are located at (−130.0 m, 10.0 m, 90.0 m). This analysis has been done with a transmitter that emits a tone of frequency 1300 MHz and a power of 7.42 Kw considering reflection and diffraction effects for the GTD analysis.

The analysis of the Doppler spectra has been run in a 2.6 GHz AMD Opteron with 256 GB of RAM, using 16 processors and obtaining the graphics shown in Figures 19 and 20. Both graphics represent the absolute value of the complex spectral response in dBV/(mHz).

5. Conclusions

To undertake the analysis of possible interferences caused by a wind turbine, three different parameters have been examined (scattered field, RCS, and Doppler shift), applying asymptotic techniques as well as rigorous techniques included in NewFasant [20]. Additionally, for the computation of the scattered field, two different geometrical models of the wind turbine have been built: a conductor and a dielectric models. Even though results obtained for the dielectric model are more realistic than results obtained for the conductor model, they still show in general a good agreement. However, the computation of the dielectric model expends more CPU time and memory than the computation of the conductor model. Therefore, the analysis of the scatter field of a real wind turbine can be performed using a conductor model in system studies. To characterize the RCS of a wind turbine, the results for the scatter map and for the bistatic RCS have been presented. Finally, the study is completed with the computation of the Doppler spectra.

Before installing a wind farm in a specific location, it is necessary to undertake a study of the impairment caused to telecommunication systems in its vicinity analyzing the scatter field, the RCS, and the Doppler shift as it has been presented in this paper. Therefore, these results may be used as a guideline to predict these interferences. This kind of study will serve to conclude whether or not it is possible to install the wind farm.

Acknowledgments

This work has been supported in part by the Comunidad de Madrid Project S-2009/TIC1485, the Castilla-La Mancha Project PPII10-0192-0083, the Spanish Department of Science, Technology Projects TEC2010-15706 and CONSOLIDER-INGENIO no. CSD-2008-0068, and a contract from NewFasant.

References

[1] http://www.ren21.net/.

[2] D. de la Vega, O. Grande, N. Cau et al., "Empirical evaluation of the impact of wind turbines on DVB-T reception quality," *IEEE Transactions on Broadcasting*, vol. 58, no. 1, pp. 1–9, 2012.

[3] K. H. Cavcey, L. Y. Lee, and M.A. Reynolds, "Television interference due to electromagnetic scattering by the MOD-2 wind turbine generators," *IEEE Transactions on Power Apparatus and Systems*, vol. 103, no. 2, pp. 407–412, 1984.

[4] D. L. Sengupta and T. B. A. Senior, "Electromagnetic interference to television reception caused by horizontal axis windmills," *Proceedings of the IEEE*, vol. 67, no. 8, pp. 1133–1142, 1979.

[5] Y. Zhang, A. Huston, R. D. Palmer, R. Albertson, F. Kong, and S. Wang, "Using scaled models for wind turbine EM scattering characterization: techniques and experiments," *IEEE Transactions on Instrumentation and Measurement*, vol. 60, no. 4, pp. 1298–1306, 2011.

[6] International Telecommunication Union, "Assessment of impairment caused to television reception by a wind turbine," Rec. ITU-R BT.805, 1992.

[7] International Telecommunication Union, "Assessment of impairment caused to digital television reception by a wind turbine," Rec. ITU-R BT.1893, May 2011.

[8] A. Tayebi, J. Gómez, I. González et al., "Performance comparison between rigorous and asymptotic techniques applied to the analysis of wind turbines," *Applied Computational Electromagnetics Society Journal*, vol. 26, no. 2, pp. 115–122, 2011.

[9] A. Naqvi, S. T. Yang, and H. Ling, "Investigation of doppler features from wind turbine scattering," *IEEE Antennas and Wireless Propagation Letters*, vol. 9, pp. 485–488, 2010.

[10] R. Bhalla, H. Ling, S. W. Lee, and D. J. Andersh, "Dynamic simulation of Doppler spectra of targets using the shooting and bouncing ray technique," *Microwave and Optical Technology Letters*, vol. 7, no. 18, pp. 840–842, 1994.

[11] E. Van Lil, D. Trappeniers, J. De Bleser, and A. Van de Capelle, "Computations of radar returns of wind turbines," in *Proceedings of the European Conference on Antennas and Propagation*, pp. 3727–3731, Berlin, Germany, March 2009.

[12] B. Lewke, F. Krug, and J. Kindersberger, "MoM based EMI analysis on large wind turbine GSM 900 MHz communication backup-system," in *Proceedings of the 18th International Zurich Symposium on Electromagnetic Compatibility (EMC '07)*, pp. 183–186, September 2007.

[13] D. Trappeniers, E. Van Lil, and A. Van de Capelle, "Effects of objects with moving parts like wind turbines on maritime RF safety and navigation systems," in *Proceedings of the European Conference on Antennas and Propagation (EuCAP '06)*, H. Lacoste and L. Ouwehand, Eds., p. 304.1, Nice, France, November 2006, (ESA SP-626).

[14] C. Morlas, M. Fares, and B. Souny, "Wind turbine effects on VOR system performance," *IEEE Transactions on Aerospace and Electronic Systems*, vol. 44, no. 4, pp. 1464–1476, 2008.

[15] B. M. Kent, K. C. Hill, A. Buterbaugh et al., "Dynamic radar cross section and radar doppler measurements of commercial general electric windmill power turbines part 1: predicted and measured radar signatures," *IEEE Antennas and Propagation Magazine*, vol. 50, no. 2, pp. 211–219, 2008.

[16] J. T. Moore, A. D. Yaghjian, and R. A. Shore, "Shadow boundary and truncated wedge ILDCs in Xpatch," in *Proceedings of IEEE Antennas and Propagation Society International Symposium*, pp. 10–13, July 2005.

[17] M. Domingo, F. Rivas, J. Perez, R. P. Torres, and M. F. Cátedra, "Computation of the radar cross section of complex bodies modeled using NURBS surfaces," *IEEE Antennas and Propagation Magazine*, vol. 37, pp. 36–47, 1995.

[18] C. de Boor, *A Practical Guide to Splines*, Springer, 1978.

[19] G. Farin, *Curve and Surfaces for Computer Aided Geometric Design*, Academic Press, San Diego, Calif, USA, 1988.

[20] http://www.fasant.com/.

[21] R. F. Harrington, *Field Computation by Moment Methods*, Macmillan, New York, NY, USA, 1968.

[22] C. Delgado E García, I. González, L. Hernandez, and F. Cátedra, "A comparison of the computational resources required by a Domain Decomposition approach and other efficient numerical techniques based on the moment method," in *Proceedings of the 6th European Conference on Antennas and Propagation (EUCAP '12)*, pp. 278–282, Prague, Czech, March 2012.

[23] E. García, C. Delgado, I. Gonzalez, J. Moreno, and F. Cátedra, "Efficient iterative solution of problems using characteristic basis function method combined with multilevel fast multipole algorithm," in *Proceedings of the 6th European Conference on Antennas and Propagation (EUCAP '12)*, pp. 211–214, Prague, Czech, March 2012.

[24] R. G. Kouyoumjian and P. H. Pathak, "A uniform geometrical theory of diffraction for an edge in a perfectly conducting surface," *Proceedings of the IEEE*, vol. 62, no. 11, pp. 1448–1461, 1974.

[25] P. H. Pathak, "Techniques for high frequency problems," in *Antenna Handbook—Theory, Applications and Design*, Y. T. Lo and S. W. Lee, Eds., chapter 4, Van Nostrand Reinhold, New York, NY, USA, 1988.

[26] J. B. Keller, "Geometrical theory of diffraction," *Journal of the Optical Society of America*, vol. 52, pp. 116–130, 1962.

[27] J. B. Keller, "Diffraction by a convex cylinder," *IRE Transactions on Antennas and Propagation*, vol. 24, pp. 312–321, 1956.

[28] D. A. McNamara, C. W. I. Pistorius, and J. A. G. Maherbe, *Introduction to the Uniform Geometric Theory of Diffraction*, Artech House, Norwood, Mass, USA, 1990.

[29] L. Lozano, O. Gutiérrez, I. González, and M. F. Cátedra, "Fast ray-tracing for computing N-bounces between flat surfaces at indoor/outdoor propagation," in *Proceedings of the International Conference on Electromagnetics in Advanced Applications*, pp. 112–115, 2007.

[30] G. A. Deschamps, "Ray techniques in electromagnetics," *Proceedings of the IEEE*, vol. 62, no. 9, pp. 1022–1035, 1972.

[31] J. A. Stratton, *Electromagnetic Theory*, McGraw-Hill, New York, NY, USA, 1941.

[32] A. Michaeli, "Equivalent edge currents for arbitrary aspects of observation," *IEEE Transactions on Antennas and Propagation*, vol. 32, no. 3, pp. 252–258, 1984.

[33] F. Cátedra, L. Lozano, I. González, E. García, and M. J. Algar, "Efficient techniques for accelerating the ray-tracing for computing the multiple bounce scattering of complex bodies

modeled by flat facets," *Applied Computational Electromagnetics Society Journal*, vol. 25, pp. 395–409, 2010.

[34] F. E. Nathason, *Radar Design Principles*, Mc-Graw Hill, New York, NY, USA, 1969.

[35] R. Hynes and R. E. Gardner, "Doppler spectra of S-band and X-band signals," *IEEE Transactions on Aerospace and Electronic Systems*, vol. 3, pp. 356–365, 1967.